Adhesion and nonwetting-wetting transition in the Al/α-Al_2O_3 interface

Qing Zhang, Tahir Çağın, Adri van Duin, and William A. Goddard III
Materials and Process Simulation Center (MSC), California Institute of Technology, Pasadena, California 91125, USA

Yue Qi and Louis G. Hector, Jr.
General Motors Research and Development Center, Warren, Michigan 48090, USA

(Received 12 August 2003; published 30 January 2004)

Using a reactive force field (ReaxFF), we investigated the structural, energetic, and adhesion properties, of both solid and liquid Al/α-Al_2O_3 interfaces. The ReaxFF was developed solely with *ab initio* calculations on various phases of Al and Al_2O_3 and Al-O-H clusters. Our computed lattice constants, elastic constants, surface energies, and calculated work of separation for the solid-solid interface agree well with earlier first-principles calculations and experiments. For the liquid-solid system, we also investigated the nonwetting-wetting transition of liquid Al on α-$Al_2O_3(0001)$. Our results revealed that the evaporation of Al atoms and diffusion of O atoms in α-Al_2O_3 lead to the wetting of liquid Al on the oxide surface. The driving force for this process is a decrease in interfacial energy. The nonwetting-wetting transition was found to lie in the 1000–1100 K range, which is in good agreement with sessile drop experiments.

DOI: 10.1103/PhysRevB.69.045423 PACS number(s): 68.08.−p, 68.35.−p, 64.90.+b

I. INTRODUCTION

The Al/α-Al_2O_3 interface is of great scientific and technological significance due the important role it plays in such diverse applications as metal-ceramic composites, metal-ceramic joints, casting and smelting processes, microelectronics, corrosion/wear protection, and coating technology.[1–7] As a consequence, this system has attracted a substantial amount of interest from experimentalists who have largely focused on the measurement and analysis of wetting and adhesion strength of liquid Al on an α-Al_2O_3 surface via the sessile drop method.[1,2,7–15] An interesting phenomenon associated with this system is that molten Al wets α-Al_2O_3 above 1150 K, but the Al/α-Al_2O_3 system remains nonwetting below 1150 K.[1] In the experiments, the wetting state is nonequilibrium, since Al metal tends to oxidize with environmental O_2 to form the Al_2O_3 solid phase. It has been argued that since the oxidation of Al influences the thermodynamics of the system, it affects the wetting behavior as well. However, some recent experiments showed that Al oxidation does not play a major role in Al wetting of α-Al_2O_3, and the primary cause for the wetting transition is the decrease in the Al/α-Al_2O_3 interfacial energy.[12] Some experimental results indicated that the formation of an oxygen-rich interphase at the liquid Al/α-Al_2O_3 interface leads to a decrease in the interfacial energy.[2] Although there are fewer experimental studies of adhesion of the solid-solid Al/α-Al_2O_3 interface than those of the corresponding liquid-solid system, high resolution transmission electron microscopy (TEM) of epitaxially grown Al on α-Al_2O_3 has revealed an atomically sharp interfacial structure.[4]

Recently, several first-principles density functional theory studies have been carried out to investigate the detailed atomic structure and energetic properties of the metal/Al_2O_3 interface.[5–7,16–20] For example, Zhang and Smith[5] found the composition of the stable Al/α-Al_2O_3 interface tovary significantly with oxygen chemical potential. Batyrev and Kleinman[7] investigated adhesion of Al(111)/α-$Al_2O_3(0001)$ and Cu(111)/α-$Al_2O_3(0001)$. Siegel *et al.*[6] employed *ab initio* computations to determine the atomic structure and work of separation (or ideal work of adhesion) for the Al(111)/α-$Al_2O_3(0001)$ interface with both Al-terminated and O-terminated α-$Al_2O_3(0001)$. A force field, which treats the electrostatic interaction associated with charge transfer, was developed by Streitz and Mintmire[21] and used in a molecular dynamics (MD) study of the solid Al/Al_2O_3 interface. They observed that O atoms rapidly diffuse into the Al lattice, resulting in a highly disordered region at the interface,[22] which is not comparable with experiments.[4] The Streitz-Mintmire potential was also used to investigate the properties of Al_2O_3 surfaces, γ-Al_2O_3, oxidation of Al metal, and other critical problems.[23–25] A significant deficiency of this force field is that it predicts the ground state of Al_2O_3 as the bixbyite structure with lower energy than the corundum structure.[26] Wilson *et al.* offered an explanation for this behavior that was centered around the exclusion of the polarizability of the O^{2-} ions in the model potentials.[27] The reactive force field (ReaxFF) approach of Duin *et al.*[28] is sufficiently general enough to describe both metallic and ionic bonds between Al and O, and is therefore well suited for use in MD simulations of Al/α-Al_2O_3. Unlike earlier force fields, ReaxFF is based solely on first-principles quantum mechanical calculations, correctly describes charge transfer (empirical force fields with fixed atomic charges are clearly inappropriate for this system), chemical reactions, and physical properties of Al, α-Al_2O_3, and Al/α-Al_2O_3, and predicts the right ground state for α-Al_2O_3.

In the present work, we investigate adhesion in solid-solid and liquid-solid Al/α-Al_2O_3 interfaces, using MD with the ReaxFF that was developed for this system. We are especially interested in examining the role of temperature in the nonwetting to wetting transition in the liquid-solid system and chose the MD simulation approach to facilitate separation of temperature and oxygen partial pressure effects in the

nonwetting to wetting transition at the Al/α-Al_2O_3 interface. The paper is organized as follows. Section II describes the development of the reactive force field for Al and α-Al_2O_3. The calculated results of the solid/solid interface with ReaxFF are presented in Sec. III. In Sec. IV, we present our MD simulation results of the liquid/solid Al/α-Al_2O_3 interface, focusing on Al wetting of the α-Al_2O_3 surface, where we also describe a simulation method used to determine the contact angle and critical temperature of the nonwetting to wetting transition. In Sec. V we summarize the major results of the paper.

II. REACTIVE FORCE FIELD FOR Al AND α-Al_2O_3

The reactive force field framework was initially developed for hydrocarbons.[28] Since then it has been successfully employed in the study of Si/SiO_2 interfaces[29] and is currently being applied to metal oxides and reactions between high energy density materials. With the ReaxFF formalism one can accurately describe bond formation, bond breaking, and charge transfer. All force field parameters were developed using the results of *ab initio* calculations. In this study, we optimized the force field parameters for Al and Al_2O_3 within the ReaxFF scheme. First and foremost, the ReaxFF parameters for Al and Al_2O_3 are fully transferable: they may be used not only for the metal/oxide interface, but also for studying the oxidation of Al and the hydration of α-Al_2O_3, and how Al or Al_2O_3 interacts/reacts with Si, SiO_2, hydrogen, hydrocarbons, and other organic molecules for which the parametrization is available.

The total energy expression for the Al and α-Al_2O_3 ReaxFF is a summation of electrostatic (Coulomb), bond, overcoordination, and van der Waals energies:

$$E_{system}=E_{Coulomb}+E_{bond}+E_{over}+E_{vdWaals}. \qquad (1)$$

The Coulomb interactions in our ReaxFF were calculated between all atom pairs with the atomic charges: these are determined for each configuration using the electron equilibration method (EEM) approach.[30] We optimized the EEM parameters (electronegativity χ, chemical hardness J, and shielding radius r) to reproduce the charge distributions of numerous clusters involving Al, O, and H calculated with an *ab initio* quantum mechanical (QM) method using the JAGUAR code.[31] The Al-O-H clusters were chosen to represent various bonding environments of Al and O with H, so this force field is transferable to situations where reactions of H and H_2O with Al and α-Al_2O_3 are of interest. The EEM parameters for O and H were determined in previous studies,[28] so we only allowed the parameters for Al to vary in our optimization. A summary of the results is listed in Table I, which clearly shows that our ReaxFF agrees well with QM results.

Unlike the ReaxFF for hydrocarbon molecules, the total valence energy includes only bond stretch terms for Al and α-Al_2O_3. It does not include angle bending and torsion terms as these are all set to zero. The parameters for the bond, overcoordination, and van der Waals energies of Al-Al and Al-O were determined by fitting the QM calculations to an equation of state of pure Al and α-Al_2O_3. For Al we fitted various crystal phases of Al, including fcc (12), hcp (12), bcc (8), sc (6), and diamond (4), which effectively allowed us to vary the coordination number of Al. In *ab initio* calculations on our periodic systems, we employed the generalized gradient approximation Perdew-Burke-Ernzerhof functional[32] and pseudopotentials[33] implemented in the CASTEP code.[34] The energy versus volume curves for various phases of Al and α-Al_2O_3 were plotted in Fig. 1; for fcc Al and α-Al_2O_3, we also give the pressure versus volume relation. Equation of state fits indicate that the force field can describe the atomic interactions for all pressures up to 400 GPa. Table II shows the computed physical properties, such as the cohesive energy (E_c), lattice parameter (a_0), bond length in Al_2O_3, bulk modulus (B), vacancy formation energies (E_{vf}), and surface energies (γ_s) of Al and α-Al_2O_3 from the force fields. These properties compare favorably with QM and experimental values. As a further test of our force field, we determined the energies and volumes of other phases for Al and Al_2O_3; the results are summarized in Table III. Notice that, the ReaxFF correctly predicts the bixbyite as a higher energy structure (compared to α-Al_2O_3), which is in agreement with QM results and the fact that the bixbyite structure is not observed from experiment. This is a significant improvement over the force fields developed by Streitz and Mintmire.[21] Although the EEM method in this work is similar to the charge equilibriation (QEq) method[42] used in the electrostatic (ES)+embedded-atom method potential,[21] we believe that our fitting procedure of various phases of Al, Al_2O_3, and Al-O-H clusters allowed ReaxFF to accurately reproduce the charge on Al and O in different bonding environments. This makes α-Al_2O_3 the most energetically favorable structure. It should be noted that the charges of Al and O in α-Al_2O_3 calculated from ReaxFF are $+0.76$ and -0.51, respectively, which agree very well with the QM results of $+0.73$ and -0.49, respectively.[6] The reader is referred to Refs. 28 and 29 for additional details on ReaxFF construction.

III. SOLID/SOLID INTERFACE

We first studied the solid/solid Al/α-Al_2O_3 interface with our reactive force field and compared the results with first-principles results as another check of the quality of our force field. Based on the crystallographic considerations and experimental observations,[4] the preferred orientation at the Al/α-Al_2O_3 interface is given by the close-packed planes (0001) α-Al_2O_3/(111) Al and $[10\bar{1}0]$ α-Al_2O_3/$[\bar{1}10]$ Al. The unit cell parameters in the directions $(2a/3)[10\bar{1}0]$ α-Al_2O_3 and $[\bar{1}10]$ Al are 2.760 and 2.835 Å, respectively, leading to a 2.7% mismatch. In this study, we considered two different stacking sequences and three different oxide terminations, for a total of six interfacial geometries. The stacking sequence differs in the position of the O layer in α-Al_2O_3 with respect to the Al(111) surface. In the fcc stacking sequence, the atoms in the Al (111) surface layer sit atop the Al surface atoms in the oxide; in the hcp stacking, the metal atoms sit atop the second O layer of oxide. Note that the α-Al_2O_3(0001) surface can be terminated with a single Al layer, a double Al layer, or an O layer. In the simulations, we

TABLE I. The calculated charges for some Al-O clusters from ReaxFF compared with QM results. The notes in parentheses give the environment of the atoms, e.g., O (OH) means O in the -OH environment. The unit of charge is in electrons.

Clusters	Atoms	Charge QM	Charge FF
$(HO)AlO_2Al(OH)$	Al	1.009	1.135
	O (OH)	−0.631	−0.724
	O (between two Al)	−0.701	−0.734
$O{=}Al{-}O{-}Al(OH)_2$	O (terminal)	−0.811	−0.508
	Al (between two O)	1.337	0.947
	O (between two Al)	−1.175	−1.846
	Al (link with OH)	1.716	1,223
	O (OH)	−0.865	−0.745
$(OH)_2Al{-}Al(OH)_2$	Al	1.046	0.800
	O	−0.852	−0.743
$(OH)_2Al{-}O{-}Al(OH)_2$	Al	1.692	1.223
	O	−1.194	−0.841
	O (OH)	−0.866	−0.746
$O(AlO_2)_2$	Al	1.653	1.071
	O (center)	−1.167	−0.944
	O (AlO_2)	−0.534	−0.306
$O(AlO_2)_3$	Al	0.965	0.964
	O (center)	−0.739	−0.954
	O (AlO_2)	−0.360	−0.319
$O(AlO_2)_4$	Al	0.827	0.933
	O (center)	−0.755	−1.309
	O (AlO_2)	−0.335	−0.316
$Al(OH)_3(H_2O)_3$	Al	1.396	0.973
	O (H_2O)	−0.621	−0.642
	O (OH)	−0.882	−0.688

used sandwich models, e.g., one Al-terminated model was constructed by stacking 3 Al-O-Al layers of α-Al_2O_3 (half of the unit cell), an Al slab with either 7 (for fcc site) or 5 (for hcp site) layers of Al(111) planes, and another 3 Al-O-Al layers of α-Al_2O_3. Periodic boundary conditions were imposed in all three directions.

We used two steps to estimate the work of separation and interfacial energy. The total energy was first calculated for various separations as the rigid slabs were brought closer together. This led to an estimate of the equilibrium interfacial separation, D_0. We then relaxed all of the atomic positions to obtain the optimized interfacial structure at 0 K, starting from the models with the computed equilibrium separations. We employed both classical molecular dynamics calculations using ReaxFF, and density functional theory (DFT) QM calculations with SEQQUEST[43] (using a Gaussian-based linear combination of atomic orbitals method) on the same configurations for comparison. The equilibrium separations for the interfaces from reactive force fields and DFT calculations are summarized in Table IV and show good agreement. After relaxation, the Al-O bond lengths near the interface decrease from those in the bulk system, but no atom migration or interdiffusion has been observed and the interfaces between Al/α-Al_2O_3 remain very sharp. The work of separation, W_{sep}, reported in Table IV was computed via

$$W_{sep} = \sigma_{Al_2O_3\text{-}sv} + \sigma_{Al\text{-}sv} - \sigma_{Al/Al_2O_3} = (E^{tot}_{Al_2O_3\text{-slab}} + E^{tot}_{Al\text{-slab}} - E^{tot}_{Al_2O_3\text{-}Al})/2A, \quad (2)$$

where $\sigma_{Al_2O_{3\text{-}sv}}$, $\sigma_{Al\text{-}sv}$ are solid-vapor surface energies, σ_{Al/Al_2O_3} is interface energy; $E^{tot}_{Al\text{-slab}}$ and $E^{tot}_{Al_2O_3\text{-slab}}$ are the total energies for the Al and α-Al_2O_3 slab, respectively, $E^{tot}_{Al_2O_3\text{-}Al}$ is the total energy for the sandwich model, and A is the interfacial area. The calculated work of separation from ReaxFF is also compared with previous QM results (see Table IV). It can be seen that the predicted D_0 values from our ReaxFF are reasonably close to the corresponding QM values for all but the double-layer Al-terminated interface where a difference of 0.79 Å is noted. Experiments indicate that the single-layer Al-terminated α-Al_2O_3 (0001) surface is the most stable.[44,45] For the Al/Al_2O_3 interface, the experi-

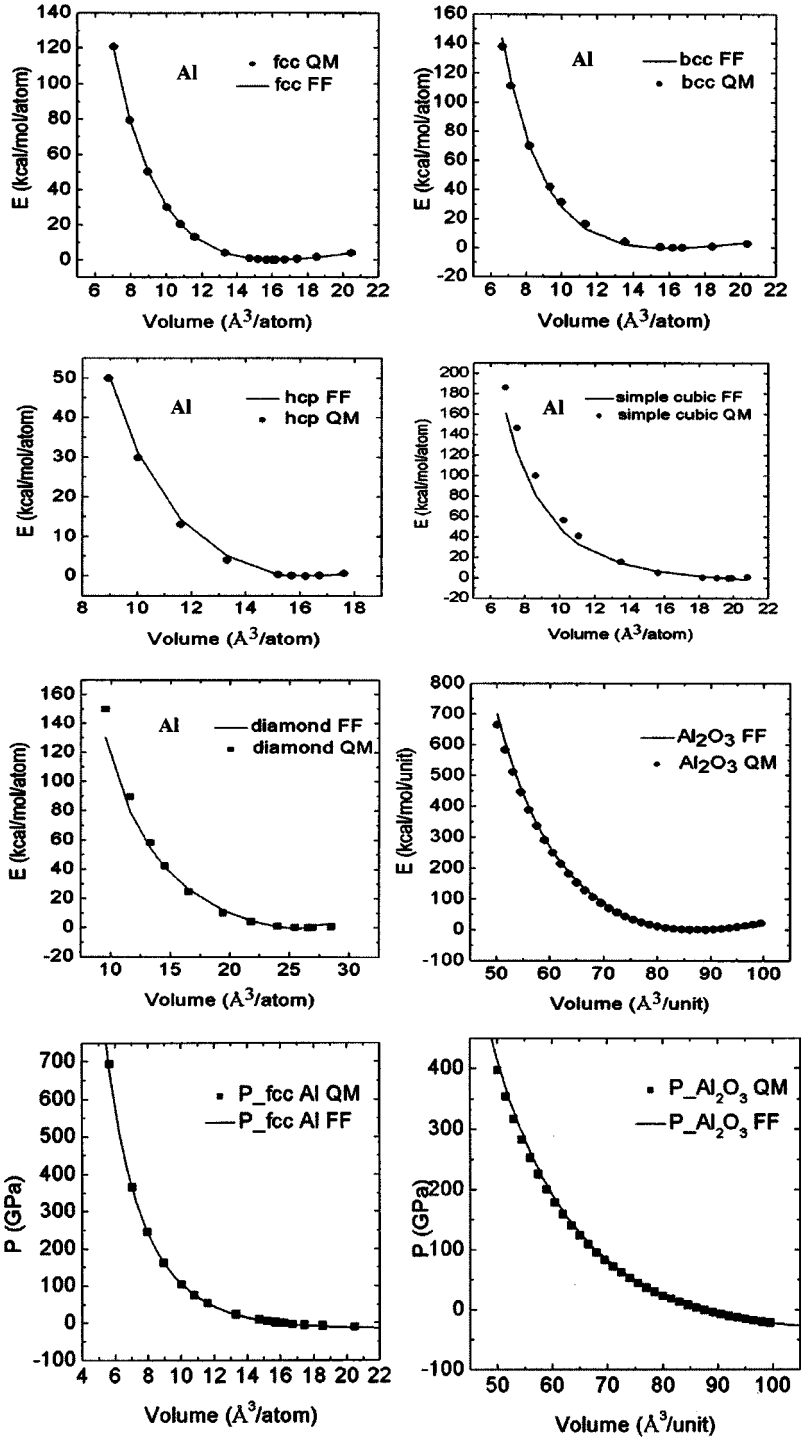

FIG. 1. Equations of state for Al metal and α-Al_2O_3. Solid lines, ReaxFF; circles, QM.

mental adhesion energy is 1.13 J/m^2,[46] which is closely reproduced by both the QM and ReaxFF calculations on the single-layer Al-terminated structure, suggesting that this type of interface is the most physically realistic for use in our calculations. On the other hand, the W_{sep} values for the O-terminated interfaces are substantially larger than those for the Al-terminated interfaces since this termination is thermodynamically unstable. Similar conclusions were reported from the results obtained using QM DFT methods by Siegel *et al.*[6] and Batyrev and Kleinman.[7]

IV. LIQUID/SOLID INTERFACE

Sessile drop experiments have revealed that molten Al on α-Al_2O_3 exhibits a nonwetting to wetting transition around 1150 K.[1] However, the origin of this transition is not clear, since there is almost always some oxidation of the molten Al droplet in these experiments. It has been suggested that Al oxidation can be neglected during the wetting process[12] and that temperature controls the transition. Accordingly, in the present MD simulations, we examined the mechanisms of the Al wetting transition at different temperatures without the

TABLE II. Physical and structural properties of (a) Al-metal QM and ReaxFF are from this work, and (b) Al_2O_3 (bl denotes bond length).

(a)

	E_c (eV)	a_0 (Å)	B (GPa)	C_{11} (GPa)	C_{12} (GPa)	C_{44} (GPa)	E_{vf} (eV)	γ_s (mJ/m^2)
QM	3.30	4.016	80					810
Expt.	3.36[a]	4.05[b]	79	114[c]	61.9	31.6	0.68[d]	980[e]
ReaxFF	3.04	4.012	78	119	57	50	0.85	576

(b)

	E_c (eV)	a (Å)	c (Å)	$\gamma(0001)$ (J/m^2)	B (Gpa)	bl $1_{Al\text{-}O}$ (Å)	bl $2_{Al\text{-}O}$ (Å)
Expt.	32[a]	4.758[f]	12.991		253[g]	1.856	1.969
QM	31	4.783	13.252	1.59	250	1.866	2.001
ReaxFF	38	4.810	13.100	1.0	248	1.890	1.965

[a]Reference 35.
[b]Reference 36.
[c]Reference 37.
[d]Reference 38.
[e]Reference 39.
[f]Reference 40.
[g]Reference 41.

influence of environmental oxygen. We employed the *NVT* (constant temperature/constant volume) MD method on the Al/α-Al_2O_3 system in vacuum. The temperature was kept constant using the Berendsen thermostat.[47] The equations of motion were solved with the Verlet algorithm using a time step of 0.5 fs. We used two models to study the wetting process, viz., a droplet model and a sandwich model.

In the droplet model, we adopted $[10\bar{1}0]$ and $[11\bar{2}0]$ as the x and y directions, respectively, for α-Al_2O_3 (0001), so the angle between the x and y axes was 90° rather than 120°. A $4\times8\times1$ superlattice slab ($33.13\times38.26\times13.25$ Å) with 1920 atoms was constructed, and 10 layers of Al(001) planes were stacked on top of the α-Al_2O_3(0001) slab. The dimensions of the Al(001) slab were $20.05\times20.05\times20.05$ Å, giving a total of 500 atoms. Periodic boundary conditions were applied in all three directions. In the z direction (perpendicular to the slab), the model was separated with a suitable vacuum region from its periodic images.

We equilibrated the model at different temperatures for 50–100 ps. Figures 2(a) and 2(b) show two snapshots of atomic structure of the Al/α-Al_2O_3 system during the equilibration at 1250 K, at $t=2$ ps and at $t=100$ ps. At $t=2$ ps, the Al slab melted and formed a liquid drop, which loosely adhered to the α-Al_2O_3 surface, showing a nonwetting configuration. After running the simulation to 100 ps, the Al atoms spread over the α-Al_2O_3 surface as shown in Fig. 2(b). This is indicative of the fact that liquid Al metal wets the α-Al_2O_3 slab at later stages of the simulation. It should be noticed that in Fig. 2(b), some Al atoms were evaporated from the Al-liquid cluster and attached at the bottom surface of the Al_2O_3 slab due to the periodic boundary condition.

The wetting process is more clearly analyzed by the variation of the density of atoms along the z direction of the Al/α-Al_2O_3 structure (Fig. 3). The outermost layer of the oxide phase is Al terminated, but these terminal Al atoms have relaxed inward to the adjacent O layer. The α-Al_2O_3 surface is around 33 Å along z, denoted by a vertical line in the insets. At $t=2$ ps, a few of the Al atoms are adsorbed on the oxide surface, which is represented by the density peak of molten Al adjacent to solid α-Al_2O_3 surface. Above the adhered layer of Al at the α-Al_2O_3 surface, there is a gap

TABLE III. Metastable phases for Al and Al_2O_3, energy in kcal/mol/atom for Al, kcal/mol/unit for Al_2O_3, volume in Å^3/atom for Al, Å^3/unit for Al_2O_3. QM results are from this work unless those noted. ΔE is the energy difference with respect to the equilibrium phase (fcc for Al and α phase for Al_2O_3).

	Al metal								Al_2O_3			
	bcc		hcp		Simple cubic		Diamond		θ		Bixbyite	
	ΔE	V	ΔE	V	ΔE	V	ΔE	V	ΔE	V	ΔE	V
QM	2.088	16.65	0.242	16.16	7.58	19.77	15.62	26.92	8.76[a]	47.9	22.37[a]	45.5
ReaxFF	1.268	15.80	0.013	16.15	8.59	22.43	16.25	25.45	4.38	51.2	15.21	49.5

[a]Reference 26.

TABLE IV. The equilibrium separation D_0 (unrelaxed) and the work of separation W_{sep} (following relaxation) for Al/Al_2O_3 interface.

	fcc-1Al	fcc-2Al	fcc-O	hcp-1Al	hcp-2Al	hcp-O
D_0 (Å) QM (this work)	2.514	2.42	1.447	2.336	2.06	1.405
D_0 (Å) ReaxFF	2.57	2.62	0.95	2.50	2.85	1.01
W_a (J/m^2) QM (this work)	1.16	1.66	8.72	1.19	2.04	9.16
W_{sep} QM	1.078[a]/1.06[b]	1.433[a]	10.095[a]/9.73[b]	0.41[b]	-	9.11[b]
W_{sep} ReaxFF	1.737	0.04	7.299	1.312	−0.177	8.074
W_{sep} Expt.	1.070[c]/1.13[d]					

[a]Reference 5.
[b]Reference 6.
[c]Reference 24.
[d]Reference 7.

between the liquid-drop region and the oxide surface; this indicates that most of the Al atoms are in the metal-drop phase and have no contact with the oxide surface. The interfacial interaction between the liquid Al and α-Al_2O_3 surface is therefore weak, and this leads to the nonwetting state. At $t=7.5$ ps, the Al and O at the α-Al_2O_3 surface merged into one layer and the Al metal atoms evaporated from the surface of the liquid drop and scattered into the vacuum domain of the simulation cell. The evaporation of Al led to an almost even density distribution of metal atoms along the z direction. Except for a few Al atoms that are adsorbed on the oxide surface, most Al atoms still have not reached the surface, denoted by the peak adjacent to the solid oxide surface and the gap between the liquid phase and the oxide surface in the metal Al density distribution curve. At $t=50$ ps, the exchange of Al and O continuously took place at the α-Al_2O_3 surface: some Al atoms at the top layer of α-Al_2O_3 diffused into the O layer and some O atoms moved outside the Al layer in the oxide. Meanwhile some of the evaporated Al metal atoms landed on the oxide surface, and the density peak of adsorbed Al atoms on the oxide surface increased substantially. (As mentioned above, some evaporated Al-metal atoms were attracted to the other side surface of α-Al_2O_3 due to the periodic boundary condition.) The gap between the adsorbed layer and the remaining Al-melt atoms vanished and the density distribution of metal Al became continuous near the interface. At the end of the 100 ps simulation time, the Al-metal atoms spread onto the surface. More importantly, interdiffusion occurred: the Al atoms in the adsorbed layer diffused into the oxide and the O atoms diffused into the liquid droplet. We observed increasing interdiffusion across the interface: For example, at $t=50$ ps about 30 Al-metal atoms diffused into O layer, and more than 80 atoms at $t=100$ ps were in the O layer, and several O atom dissolved into the liquid-Al phase from bulk α-Al_2O_3. Once the interdiffusion of Al and O started, the stoichiometry at interface changed. It can be understood from the following reaction: $Al+Al_2O_3 \rightarrow 3AlO$.

The nonwetting to wetting transition for liquid Al on an α-Al_2O_3 surface is driven by a decrease in the total energy of the system, which in turn is driven by the formation of new O-Al bonds at the interface. There are two important factors associated with this process: (1) the evaporation of Al atoms from the liquid to the α-Al_2O_3 surface, and (2) the diffusion of O from the bulk α-Al_2O_3 to the surface, which caused the α-Al_2O_3 surface to change its Al-termination to an O-rich phase. The decrease of the interfacial energy thus leads to an increase of W_{sep} and a decrease in the contact angle, which is in agreement with experimental observations.[2] Thus, an Al-rich aluminum oxide phase is formed at the interface. We have monitored and calculated the coordination number change of Al at the Al/Al_2O_3 interfacial region during the annealing at 1250 K. Figure 4 shows the variation of the average coordination of Al atoms at the interface region. In bulk Al_2O_3, the Al has 6 O neighbors and O has 4 Al neighbors. At the single-Al-terminated Al_2O_3 surface, the Al at the surface has 3 O neighbors. The interfacial region is defined as follows: starting from the outermost Al layer of the Al_2O_3 phase, we monitored the average coordination of Al atoms, layer by layer, into the oxide phase and into the metal phase. Each layer has 128 Al atoms in the oxide phase (except for the top layer, which has 64 Al at-

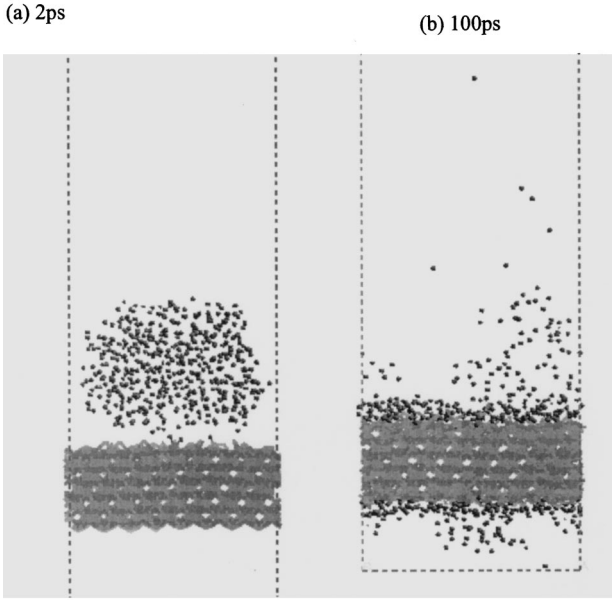

FIG. 2. Snapshots for the Al/α-Al_2O_3 interface at 1250 K running after (a) 2 and (b) 100 ps.

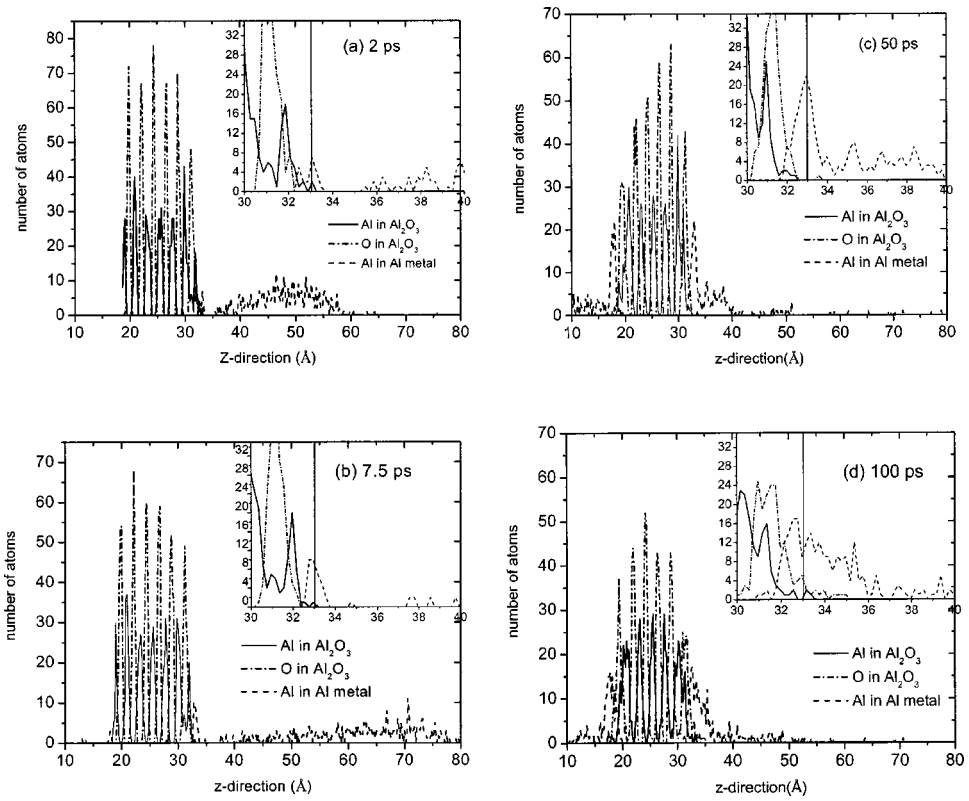

FIG. 3. Distribution of atoms along the z direction at 1250 K after (a) 2, (b) 7.5, (c) 50, and (d) 100 ps. The inset shows the distribution of a small scale at the Al/α-Al_2O_3 interface. The interface of Al_2O_3 and Al is denoted with a solid line in the inset.

oms), and 50 Al atoms in the metal phase. Considering the outermost layer of oxide phase as layer 0, at the third layer of the oxide phase even at the end of 100 ps the coordination remains 6, indicating that within this time frame the bulk α-Al_2O_3 stochiometry remains intact below the third layer. The distribution of the Al-O coordination in oxide and metal phases at the interfaces at the end of the 100 ps simulation is tabulated in Table V, along with the final average coordination (where the layer labeling is -1, -2, -3 into the oxide phase, 1, 2, 3 into the metal phase). Layer 0 Al atoms are on the average, threefold coordinated. The coordination distribution for the layer 0 at the end of 100 ps is, 4/64 twofold coordinated, 39/64 threefold coordinated, 20/64 fourfold coordinated, and 1/64 fivefold coordinated Al. In layer -1 in the oxide phase at the interface, the average coordination of Al reduces to slightly over 5 (5.37) and layers -2 and -3 are very close to 6 (5.91 and and 5.97, respectively) at the end of the 100 ps simulation. The variation of Al-O coordination for metal layers 1 through 3 is displayed in Fig. 4 and Table V. Here, one observes coordinations ranging from 0 to 4 as the simulation time increases.

Additional simulations were also performed at temperatures of 900, 1100, 1200, and 1300 K. We found that the diffusion at the interface was faster at higher temperatures than at lower temperatures, which accelerates the wetting process. This is in agreement with the experimental results that the spreading/wetting time is reduced at elevated temperatures. At 900 K, no diffusion of O was observed at 50 ps; therefore the outermost layer of oxide was still Al terminated and Al-metal atoms remained in the droplet.

The drawback to the above model simulation is that it only gave a qualitative description of nonwetting or wetting. Due to the limitations imposed by the size of model system, we were not able to determine the contact angles using this procedure as we have successfully used it in determining contact angles and surface tensions of various crystalline

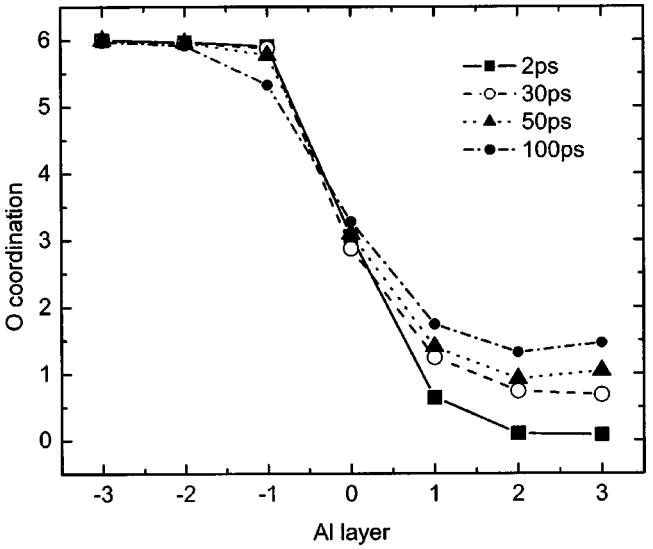

FIG. 4. The evolution of the O coordination number of Al atoms in the interfacial layers during 1250 K simulation. The 0 layer is the topmost Al layer of Al_2O_3 at the interface, -1, -2, -3 are the Al layers in Al_2O_3, and 1,2,3 are Al layers in Al metal. Layer 0 has 64 atoms, layers -1, -2, -3 each have 128 Al atoms, and metal phase layers have 50 Al atoms. The Al-O coordination plotted here is the average over the atoms of each layer. The distribution of the Al-O coordination for each layer at the end of 100 ps run is given in Table V.

TABLE V. The number of Al atoms of different O coordination at interfacial layers after annealing at 1250 K for 100 ps. The 0 layer is the Al layer of Al_2O_3 at the interface, -1, -2, -3 are Al layers in Al_2O_3, and 1, 2, 3 are Al layers in Al metal.

Coordination layer	0	1	2	3	4	5	6	Average
-3	0	0	0	0	0	4	124	5.97
-2	0	0	0	0	2	8	118	5.91
-1	0	0	0	1	16	51	60	5.36
0	0	0	4	39	20	1	0	3.28
1	15	6	7	21	1	0	0	1.74
2	18	14	3	14	1	0	0	1.32
3	17	11	7	12	3	0	0	1.40

polymers.[48] Therefore, we used an alternative model with a solid α-Al_2O_3 slab sandwiched between two slabs of liquid Al phases to estimate the contact angle and the temperature of the nonwetting-wetting transition point.

The wettability of α-Al_2O_3 by liquid Al is determined Young's equation,

$$\sigma_{\text{Al-}lv}\cos\theta+\sigma_{\text{Al/Al}_2\text{O}_3}=\sigma_{\text{Al}_2\text{O}_3\text{-}sv} \tag{3}$$

where $\sigma_{\text{Al-}lv}$ is the surface tension for the liquid-vapor interface of Al, $\sigma_{\text{Al/Al}_2\text{O}_3}$ is the interfacial tension at the boundary between liquid Al and solid α-Al_2O_3, $\sigma_{\text{Al}_2\text{O}_3\text{-}sv}$ is the surface tension for solid-vapor interface for α-Al_2O_3, and θ is the contact angle. When $\theta<90°$, the solid is wet by the liquid, and $\theta>90°$ indicates nonwetting behavior. Combining Eqs. (2) and (3) gives the familiar Young-Dupre equation

$$W_{sep}=\sigma_{\text{Al-}lv}(1+\cos\theta). \tag{4}$$

Equation (4) indicates that the lower θ and the higher $\sigma_{\text{Al-}lv}$, the larger W_{sep}, which has been confirmed by Ksiazek *et al.*[1] with a special procedure to study shear strength using sessile drop samples in the Al/α-Al_2O_3 system. The results show that the higher the wetting temperature, the lower the contact angle θ and the higher the interfacial shear strength.

Combining Eqs. (2) and (4), we obtain the following relationships:

$$2AW_{sep}=E^{\text{tot}}_{\text{Al}_2\text{O}_3\text{-slab}}+E^{\text{tot}}_{\text{Al-slab}}-E^{\text{tot}}_{\text{Al}_2\text{O}_3\text{-Al}}, \tag{5}$$

$$2A\sigma_{lv}(1+\cos\theta)=E^{\text{tot}}_{\text{Al}_2\text{O}_3\text{-slab}}+(E^{\text{tot}}_{\text{Al-}l\text{-bulk}}+2A\sigma_{lv})-E^{\text{tot}}_{\text{Al}_2\text{O}_3\text{-Al}}, \tag{6}$$

$$\cos\theta=\frac{E^{\text{tot}}_{\text{Al}_2\text{O}_3\text{-slab}}+E^{\text{tot}}_{\text{Al-}l\text{-bulk}}-E^{\text{tot}}_{\text{Al}_2\text{O}_3\text{-Al}}}{2A\sigma_{lv}}. \tag{7}$$

Above the melting temperature, the Al slab is a mixture of liquid and vapor, and it is difficult to determine the value of $E^{\text{tot}}_{\text{Al-slab}}$. Thus, in Eq. (6), we have used the total energy of bulk liquid $E^{\text{tot}}_{\text{Al-}l\text{-bulk}}$ plus the surface energy $2A\sigma_{lv}$ in place of the total energy of the liquid slab. As the liquid surface energy is depleted on both sides, the sign of $\cos\theta$ only depends on the sign of $(E^{\text{tot}}_{\text{Al}_2\text{O}_3\text{-slab}}+E^{\text{tot}}_{\text{Al-}l\text{-bulk}}-E^{\text{tot}}_{\text{Al}_2\text{O}_3\text{-Al}})$, whereas the surface energy of the liquid only influences the value of $\cos\theta$. Since both $E^{\text{tot}}_{\text{Al}_2\text{O}_3\text{-slab}}$ and $E^{\text{tot}}_{\text{Al-}l\text{-bulk}}$ are constants at the specific temperature, only the interfacial energy $E^{\text{tot}}_{\text{Al}_2\text{O}_3\text{-Al}}$ influences the sign of $\cos\theta$, which determines wetting or nonwetting at the specific simulation temperature. When $\cos\theta>0$, $\theta<90°$, and liquid Al wets the α-Al_2O_3 surface; whereas when $\cos\theta<0$, $\theta>90°$, the liquid Al does not wet the surface. It should be noted that the above equations are only satisfied when no new phases have been formed at the interface; otherwise it is necessary to account for the heat of formation of the new phase.

To determine the temperature at which the nonwetting-wetting transition occurs, we performed *NVT* simulations with the sandwich model in the 950 to 1300 K temperature range. In the sandwich model, the potential energy of the system is given by $E^{\text{tot}}_{\text{Al}_2\text{O}_3\text{-Al}}$, which was monitored in these simulations. Figure 5 shows the variation of the potential energy for the sandwich model at 1100 and 1200 K. The values of $E^{\text{tot}}_{\text{Al}_2\text{O}_3\text{-slab}}$ and $E^{\text{tot}}_{\text{Al-}l\text{-bulk}}$ at 1100 and 1200 K were calculated from the α-Al_2O_3 slab model and bulk Al-liquid model independently, and their summation is also plotted as a straight line to represent the baseline. At $T=1100$ K, the potential energy fluctuates around $E^{\text{tot}}_{\text{Al}_2\text{O}_3\text{-slab}}+E^{\text{tot}}_{\text{Al-}l\text{-bulk}}$, implying that $\cos\theta$ is almost equal to zero and representing the transition state from nonwetting to the wetting. We observe that at $T=1200$ K, the potential energy of system decreases with time. At the beginning of the simulation, the energy was higher than $E_{\text{Al}_2\text{O}_3\text{-slab}}+E_{\text{Al-}l\text{-bulk}}$, indicating nonwetting at that time. At about $t=25$ ps, the potential energy becomes less than that of $E^{\text{tot}}_{\text{Al}_2\text{O}_3\text{-slab}}+E^{\text{tot}}_{\text{Al-}l\text{-bulk}}$: this indicates that the wetting process has begun. The decrease of the potential energy is due to the migration of O atoms from the bulk oxide to the surface as discussed above. This reduces the interfacial energy and increases the work of separation. From the solid Al/α-Al_2O_3 calculation in Sec. III, we know that the O-terminated interface has a much larger W_{sep} than the Al-terminated interface.

After the wetting transition, we found that the potential energies kept decreasing at temperatures higher than 1100 K. This is because oxygen tends to continue diffusing into the Al-liquid region, so a new phase of aluminum oxide forms inside liquid Al. In Fig. 6, we show the atomic number den-

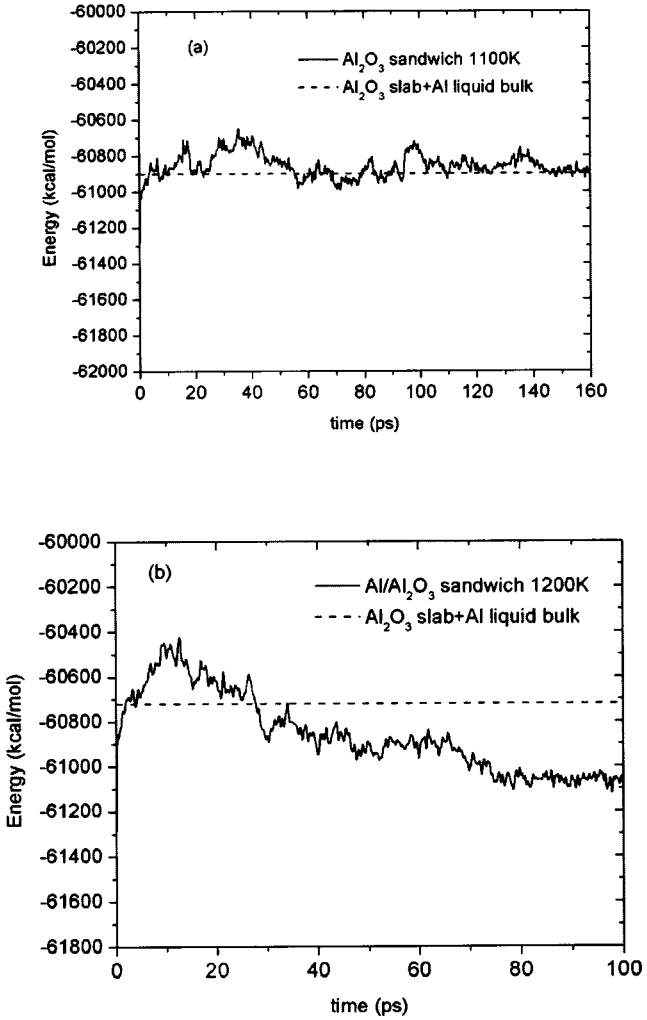

FIG. 5. Energy change with time for the sandwich model at (a) $T=1100$ and (b) $T=1200$ K. The baseline is the sum of the energy of the Al_2O_3 slab and the energy of Al-liquid bulk.

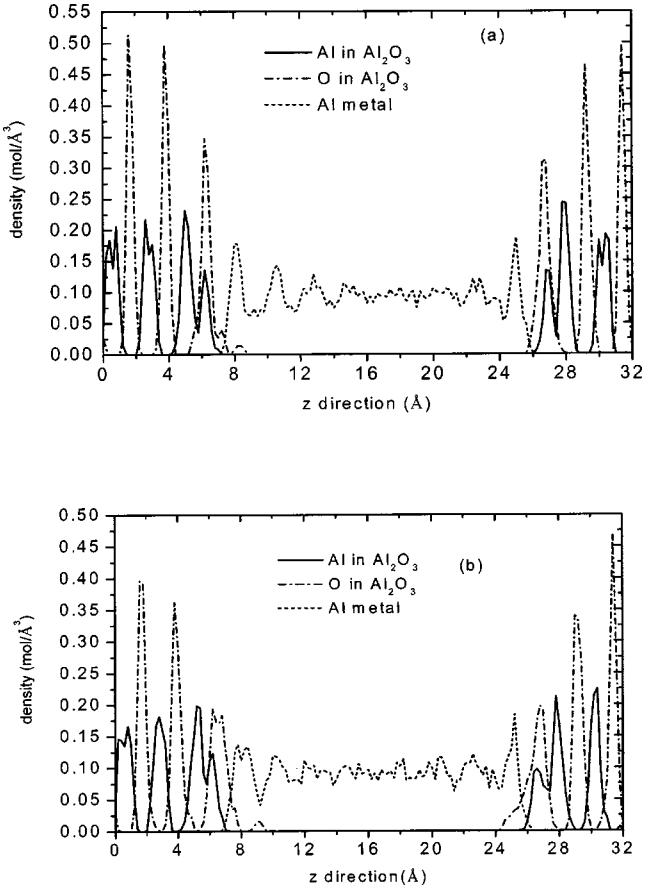

FIG. 6. Density of atoms along the z direction for an Al/Al_2O_3 sandwich model after running 100 ps at (a) $T=950$ K and (b) $T=1200$ K (averaging for 100–110 ps $\Delta z=0.2$ Å).

sity distribution along the z direction for 950 and 1200 K after running for $t_{\mathrm{sim}}=100$ ps. At $T=950$ K, almost no oxygen diffusion to the α-Al_2O_3 surface nor into liquid Al is observed: this indicates that the nonwetting state is stable at 950 K. However, at $T=1200$ K, we see that 7 atoms (up to 26% of O atoms in the first O layer of Al_2O_3) have diffused into the liquid-Al region at one side of the interface, which then formed 30 bonds with the Al metal with a bond distance of less than 2.2 Å, which indicates where new Al-O phases spread along the z direction.

To evaluate the contact angle from Eq. (7), one must use the energy without any new phase formation. However the continuous diffusion of oxygen into the Al droplet and new Al-O phase formation within liquid Al will cause the contact angle to continuously change, and Eq. (7) is not valid anymore. Therefore, we decided to only calculate the contact angle at the equilibrium state (i.e., for 950 K) or the state right after oxygen diffusion to the Al surface but not into the liquid phase. We have determined those energies for the structures at the moment just before the oxidation within liquid Al from the MD trajectory. Thus the contact angle will correspond to the structure at equilibrium or just after wetting transition.

The surface tension of the liquid Al (σ_{lv}) was calculated with the cluster method employed by us to study Ar clusters.[49] Based on this method, the potential energy of a macroscopic liquid drop can be written in terms of the number of particles in the drop (n), the chemical potential of a particle in the bulk (μ), the volume of the drop (v), the surface tension (σ), and Tolman length (δ):

$$\frac{E}{n}=\mu+\sigma(4\pi)^{1/3}(3v)^{2/3}n^{-1/3}-2\sigma\delta(4\pi)^{2/3}(3v)^{1/3}n^{-2/3}. \tag{8}$$

At different temperatures, we fit the potential energies of icosahedral clusters with different sizes to Eq. (8) to get the change in the surface tension of liquid Al with temperature. We then estimate the contact angle at different temperatures with Eq. (7), and the results compared with the experiments are shown in Table VI. The contact angle changes from 140° at 950 K to 74° at 1250 K and shows that a nonwetting to wetting transition occurs with the elevated temperature. The critical point of the nonwetting-wetting transition is within 1000–1100 K, which is close to the experimental value about 1150 K.

TABLE VI. Contact angles for the Al/Al_2O_3 interface calculated from Eq. (8) compared with experiments. The total energies and contact angles are captured at the time before O diffused into Al liquid phase (listed in the table).

Simulation			Experiment[a]	
T (K)	θ (deg)	Time (ps)	T (K)	θ (deg)
950	140	63	953	126
1000	96	66	1023	121
1100	82	70	1123	96
1200	65	46	1223	79
1250	74	33	1323	74

[a]Reference 1.

V. SUMMARY

Employing a reactive force field, we constructed the potential for Al and Al_2O_3 to reproduce the equations of state and physical properties of aluminum metal and aluminum oxides. With this force field, the work of separation of the Al/α-Al_2O_3 interface was calculated, which is in agreement with experimental and quantum mechanics results. With molecular dynamics simulations of the wetting process of liquid Al on an α-Al_2O_3 surface, it has been revealed that the evaporation of Al-metal atoms and diffusion of O atoms cause the spreading/wetting of liquid Al on the oxide surface. The formation of new Al-O bonds at interfaces leads to a decrease of the interfacial energy, which is the driving force for wetting and spreading of liquid Al. Finally, with a MD simulation model, we estimated the critical temperature of nonwetting-wetting transition of the system to lie in the 1000–1100 K range.

ACKNOWLEDGMENTS

This research is funded by General Motors. The facilities of MSC is also supported by funding from NSF, NIH, DoE, DoD, Beckman Institute and by grants from the industrial partners Avery-Dennison, Asahi Chemical, Chevron, Dow, Epson-Seiko, 3M.

[1] M. Ksiaxek, N. Sobczak, B. Mikulowski, W. Radziwill, and I. Surowiak, Mater. Sci. Eng., A **324**, 162 (2002).
[2] G. Levi and W. D. Kaplan, Acta Mater. **50**, 75 (2002).
[3] V. Gupta, A. S. Argon, and J. A. Cornie, J. Mater. Sci. **24**, 2031 (1989).
[4] D. L. Medlin, K. F. McCarty, R. Q. Hwang, S. E. Guthrie, and M. I. Baskes, Thin Solid Films **299**, 110 (1997).
[5] W. Zhang and J. R. Smith, Phys. Rev. Lett. **85**, 3225 (2000).
[6] D. J. Siegel, L. G. Hector, Jr., and J. B. Adams, Phys. Rev. B **65**, 085415 (2002).
[7] I. G. Batyrev and L. Kleinman, Phys. Rev. B **64**, 033410 (2001).
[8] N. Eustathopoulos, B. Drevet, and M. G. Nicholas, *Wettability at High Temperatures* (Pergamon, New York, 1999).
[9] H. N. Ho and S. T. Wu, Jpn. J. Appl. Phys., Part 1 **37**, 274 (1998).
[10] G. Levi and W. D. Kaplan, J. Am. Ceram. Soc. **85**, 1601 (2002).
[11] K. Landry and N. Eustathopoulos, Acta Mater. **44**, 3923 (1996).
[12] X. B. Zhou and J. T. M. de Hosson, J. Mater. Sci. **30**, 3571 (1995).
[13] V. Merlin and N. Eustathopoulos, J. Mater. Sci. **30**, 3619 (1995).
[14] D. A. Weirauch, W. M. Balaba, and A. J. Perrotta, J. Mater. Res. **10**, 640 (1995).
[15] J. Hautmann and M. Klein, Phys. Rev. Lett. **67**, 1763 (1991).
[16] Z. Lodziana and J. K. Norskov, J. Chem. Phys. **115**, 11261 (2001).
[17] A. Bogicevic and D. R. Jennison, Phys. Rev. Lett. **82**, 4050 (1999).
[18] Y. F. Zhukovskii, E. A. Kotomin, B. Herschend, K. Hermansson, and P. M. W. Jacobs, Surf. Sci. **513**, 343 (2002).
[19] I. G. Batirev, A. Alavi, M. W. Finnis, and T. Deutsch, Phys. Rev. Lett. **82**, 1510 (1999).
[20] C. Verdozzi, P. A. Schultz, R. Q. Wu, A. H. Edwards, and N. Kioussis, Phys. Rev. B **66**, 125408 (2002).
[21] F. H. Streitz and J. W. Mintmire, Phys. Rev. B **50**, 11996 (1994).
[22] F. H. Streitz and J. W. Mintmire, Compos. Interfaces **2**, 473 (1994).
[23] T. Campbell, R. K. Kalia, A. Nakano, P. Vashishta, S. Ogata, and S. Rodgers, Phys. Rev. Lett. **82**, 4866 (1999).
[24] S. Ogata and T. J. Campbell, J. Phys.: Condens. Matter **10**, 11449 (1998).
[25] F. H. Streitz and J. W. Mintmire, Phys. Rev. B **60**, 773 (1999).
[26] S. D. Kenny, D. Nguyen-Manh, H. Fujitani, and A. P. Sutton, Philos. Mag. Lett. **78**, 469 (1998).
[27] M. Wilson, M. Exner, Y. M. Huang, and M. W. Finnis, Phys. Rev. B **54**, 15683 (1996).
[28] A. C. T. van Duin, S. Dasgupta, F. Lorant, and W. A. Goddard III, J. Phys. Chem. A **105**, 9396 (2001).
[29] A. C. T. van Duin, A. Strachan, S. Stewman, Q. S. Zhang, X. Xu, and W. A. Goddard III, J. Phys. Chem. A **107**, 3803 (2003).
[30] W. J. Mortier, S. K. Ghosh, and S. Shankar, J. Am. Chem. Soc. **108**, 4315 (1986).
[31] B. H. Greeley, T. V. Russo, D. T. Mainz, R. A. Friesner, J.-M. Langlois, W. A. Goddard III, R. E. Donnelly, Jr., and M. N. Ringalda, J. Chem. Phys. **101**, 4028 (1994).
[32] J. P. Perdew, K. Burke, and M. Ernzerhof, Phys. Rev. Lett. **77**, 3865 (1996).

[33] N. Troullier and J. L. Martin, Phys. Rev. B **43**, 1993 (1991).
[34] M. C. Payne, M. P. Teter, D. C. Allan, T. A. Arias, and J. D. Joannopoulos, Rev. Mod. Phys. **64**, 1045 (1992).
[35] *Handbook of Chemistry and Physics*, edited by R. C. Weast (CRC, Boca Raton, FL, 1984).
[36] C. Kittel, *Introduction to Solid State Physics* (Wiley-Interscience, New York, 1986).
[37] G. Simons and H. Wang, *Single Crystal Elastic Constants and Calculated Aggregate Properties* (MIT Press, Cambridge, MA, 1977).
[38] H. E. Schaefer, R. Gugelmeier, M. Schmolz, and A. Seeger, Mater. Sci. Forum **15-18**, 111 (1987).
[39] L. E. Murr, *Interfacial Phenomena in Metals and Alloys* (Addison-Wesley, Reading, MA, 1975).
[40] W. H. Gitzen, *Alumina as a Ceramic Material* (The American Ceramic Society, Columbus, OH, 1970).
[41] P. Richet, J. Xu, and H. K. Mao, Phys. Chem. Miner. **16**, 207 (1988).
[42] A. K. Rappe and W. A. Goddard, J. Phys. Chem. **95**, 3358 (1991).
[43] P. A. Schultz (unpublished). For the method see P. J. Feibelman, Phys. Rev. B **35**, 2626 (1987).
[44] P. Guenard, G. Renaud, A. Barbier, and M. Gautier-Soyer, Surf. Rev. Lett. **5**, 321 (1997).
[45] A. Wander, B. Searle, and N. M. Harrison, Surf. Sci. **458**, 25 (2000).
[46] D. M. Lipkin, J. N. Israelachivili, and D. R. Clarke, Philos. Mag. A **76**, 715 (1997).
[47] H. J. C. Berendsen, J. Chem. Phys. **81**, 3684 (1984).
[48] C. F. Fan and T. Cagin, J. Chem. Phys. **103**, 9053 (1995).
[49] R. B. McClurg, R. C. Flagan, and W. A. Goddard, J. Chem. Phys. **102**, 3322 (1995).